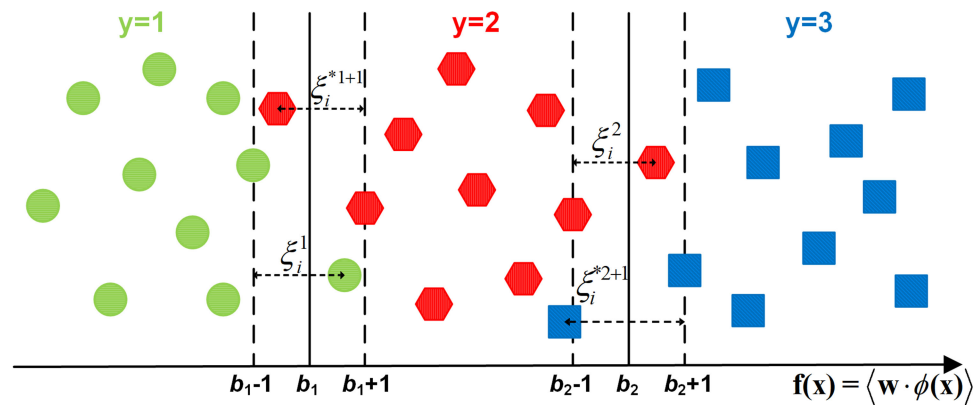


# OSNR Monitoring Using Support Vector Ordinal Regression for Digital Coherent Receivers

Volume 11, Number 5, October 2019

Ming Hao  
Lianshan Yan  
Anlin Yi  
Lin Jiang  
Yan Pan  
Wei Pan  
Bin Luo



DOI: 10.1109/JPHOT.2019.2941984

# OSNR Monitoring Using Support Vector Ordinal Regression for Digital Coherent Receivers

Ming Hao<sup>1,2</sup>, Lianshan Yan<sup>1,2</sup>, Anlin Yi<sup>1,2</sup>, Lin Jiang<sup>1,2</sup>, Yan Pan,<sup>2</sup>  
Wei Pan,<sup>2</sup> and Bin Luo<sup>2</sup>

<sup>1</sup>Artificial Intelligence Key Laboratory of Sichuan Province, Sichuan University of Science and Engineering, Yibin 644000, China

<sup>2</sup>Center for Information Photonics and Communications, School of Information Science and Technology, Southwest Jiaotong University, Chengdu 611756, China

DOI:10.1109/JPHOT.2019.2941984

This work is licensed under a Creative Commons Attribution 4.0 License. For more information, see <https://creativecommons.org/licenses/by/4.0/>

Manuscript received March 12, 2019; revised July 17, 2019; accepted September 12, 2019. Date of publication September 17, 2019; date of current version October 28, 2019. This work was supported in part by the National Natural Science Foundation of China under Grant 61860206006, in part by the 111 Plan (B18045), and in part by the Major Frontier Project of Sichuan Science and Technology under Grant 2018JY0512. Corresponding author: Lianshan Yan (e-mail: lsyan@home.swjtu.edu.cn).

**Abstract:** An OSNR monitoring method assisted by support vector ordinal regression (SVOR) is proposed for digital coherent receivers. According to Godard's error of equalized signals obtained after polarization demultiplexing, the optical signal-to-noise ratio (OSNR) value could be effectively estimated by using SVOR. The effectiveness of the proposed OSNR monitoring method is verified via numerical simulations with 28-Gbaud PDM-QPSK, PDM-8PSK, PDM-8QAM, PDM-16QAM and PDM-32QAM signals. The simulation results show that the 100% accuracies for the five modulation formats can be obtained over a wide OSNR range. The feasibility is further demonstrated by proof-of-concept experiments in 28-Gbaud PDM-QPSK, PDM-8PSK, PDM-8QAM and PDM-16QAM systems. The errors of averaged values of estimated OSNR for all the signals are less than or equal to 0.2 dB.

**Index Terms:** OSNR Monitoring, Godard's error, support vector ordinal regression.

## 1. Introduction

In order to achieve higher spectral efficiency [1] and better quality of service, flexible and programmable optical networks are needed. Thus, the elastic optical network (EON) [2] with the capability to adaptively adjust the data rate, bandwidth, modulation format and signal power according to variable traffic demand has attracted extensive attention in recent years [3]. For EON, the information about the physical state of transmission link and the quality of optical signals should be available. As an important parameter of EON, Optical signal-to-noise ratio (OSNR) should be monitored since it is one of signal quality metrics [4] and is directly related to the bit error rate (BER). Accurate OSNR monitoring could provide reasonable level of reliability of network and ensure the quality of signals [5].

Traditional OSNR monitoring methods are mainly implemented based on additional hardware components [6]–[10]. Due to the continuous progress of digital signal processing (DSP) technology, OSNR monitoring can be realized based on algorithms that embedded in the DSP module of digital coherent receiver without any additional hardware components [11]–[19], and is more flexible, cost-effective and practical. Recently, various features of digital signals detected by

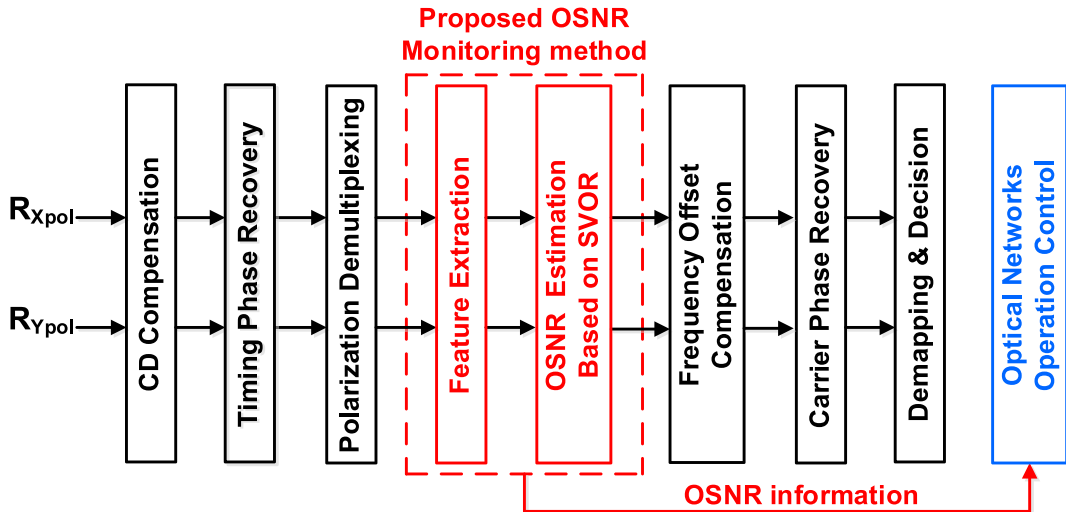


Fig. 1. DSP architecture with proposed OSNR monitoring method for digital coherent receivers.

coherent receiver have been utilized as the metric of OSNR, including statistical moment [11]–[13], error vector magnitude (EVM) [14], [15], equalized training sequence [16], cumulative distribution function (CDF) [17], amplitude histogram of equalized signals [18] and constellation diagram [19]. In fact, variation of OSNR value would cause change of intensity fluctuation of equalized signals. The intensity fluctuation feature is defined as Godard's error [20], and is widely used in chromatic dispersion equalization [21], nonlinear parameter monitoring [22], [23], and modulation format identification [24].

Actually, the evolution of the features of OSNR usually obeys a particular order. The features of OSNR are mainly confused between adjacent OSNR values. The difference of features between non-adjacent OSNR values is relatively obvious, and not easy to be confused. Therefore, the inherent ordinal information among OSNR monitoring range is another special characteristic of OSNR. As one of ordinal regression algorithms, support vector ordinal regression (SVOR) is generally used in the multiple classes case that label is ordered. Similar to support vector machine (SVM), SVOR maximizes the margin width between adjacent classes to find the optimal discriminant hyperplanes. The difference is that SVM generates only one discriminant hyperplane to distinguish two classes while SVOR generates  $M - 1$  parallel discriminant hyperplanes for  $M$  classes simultaneously. SVOR optimizes the mapping direction and multiple thresholds to define parallel discriminant hyperplanes, and the size of optimization problem is linear to the number of training vectors [25].

In this paper, an effective OSNR monitoring method using SVOR is proposed. According to Godard's error of equalized signals obtained after polarization demultiplexing, the SVOR could estimate OSNR value over a wide range. In numerical simulations, 100% accuracies are obtained for the OSNR estimation of 28-Gbaud PDM-QPSK, PDM-8PSK, PDM-8QAM, PDM-16QAM and PDM-32QAM signals. Furthermore, proof-of-concept experiments have been implemented to demonstrate the feasibility of the proposed OSNR monitoring method among 28-Gbaud PDM-QPSK, PDM-8PSK, PDM-8QAM and PDM-16QAM signals. The experimental results show that the errors of averaged values of estimated OSNR for all the signals are less than or equal to 0.2 dB.

## 2. Operating Principle

The DSP architecture with proposed OSNR monitoring method for digital coherent receivers is shown in Fig. 1. The proposed OSNR monitoring method, as shown in the red box, is placed behind the chromatic dispersion (CD) compensation, timing phase recovery and polarization demultiplexing. The proposed OSNR monitoring method consists of two steps including feature extraction and

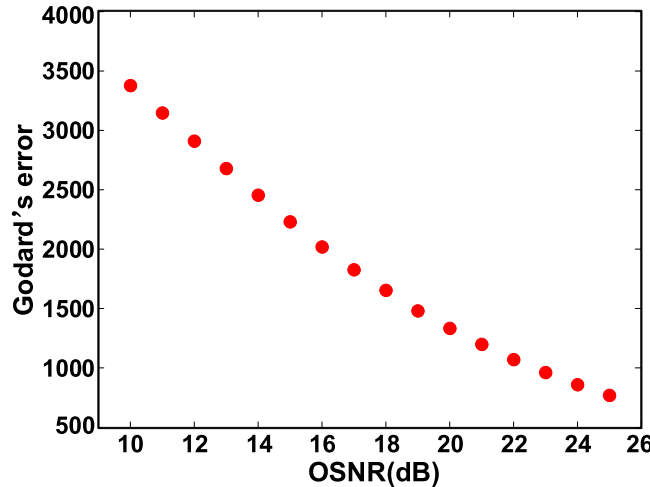


Fig. 2. Godard's error corresponding to different OSNR values for QPSK signals.

OSNR estimation based on SVOR. The estimated OSNR information is directly related to signal quality and could be applied as automatic fault detection [18]. Furthermore, the OSNR information could feedback to the networking operation decision for assisting optical network to adjust the corresponding system parameters [17].

### 2.1 Feature Extraction

Here Godard's error, which is intensity fluctuation feature, is considered as signal quality metric to monitor OSNR and defined as [20]:

$$\varepsilon_{\text{Godard}} = \sum_{n=1}^N \left( |D(n)|^2 - R \right), R = \frac{E \left\{ |D(n)|^4 \right\}}{E \left\{ |D(n)|^2 \right\}} \quad (1)$$

where  $|D(n)|^2$  is intensity of equalized signal obtained after polarization demultiplexing,  $N$  is the number of symbols,  $R$  is the constant power of signal,  $E\{\cdot\}$  indicates the expectation value. Since  $R$  is constant, Godard's error actually represents intensity fluctuation of signals relative to  $R$  as depicted in Eq. (1).

The Godard's errors corresponding to different OSNR values for QPSK signals are shown in Fig. 2, and the number of symbols is 8000. When the OSNR value is lower, the Godard's error is greater because the intensity fluctuation of equalized signals is more obvious. It can be observed that the Godard's errors corresponding to different OSNR values have certain adjacent relations. Therefore, Godard's error can be regarded as the OSNR monitoring metric. The histograms of intensity signal  $|D(n)|^2$  of five commonly used modulation formats (i.e., QPSK, 8PSK, 8QAM, 16QAM and 32QAM) at different OSNR values are shown in Fig. 3. For  $m$ QAM signals that are with multiple intensity levels, the intensity fluctuation caused by noise can't be accurately described by only one  $R$  as depicted in Eq. (1). In order to accurately describe the intensity fluctuation, thresholds of intensity depicted as vertical red dash lines in Fig. 3 are applied to divide intensity into  $k$  levels ( $k = 2$  for 8QAM,  $k = 3$  for 16QAM, and  $k = 4$  for 32QAM). Based on the thresholds, the  $R$  of each individual intensity level can be obtained, so that the Godard's error which represents the intensity fluctuation of corresponding level can be calculated. It should be noted that the intensity of 32QAM is five-levels. However, as shown in fig. 3, the fifth intensity level of 32QAM is not obvious even the OSNR rises to 30 dB. Therefore, the fourth and fifth intensity level use the same  $R$  to describe the intensity fluctuation.

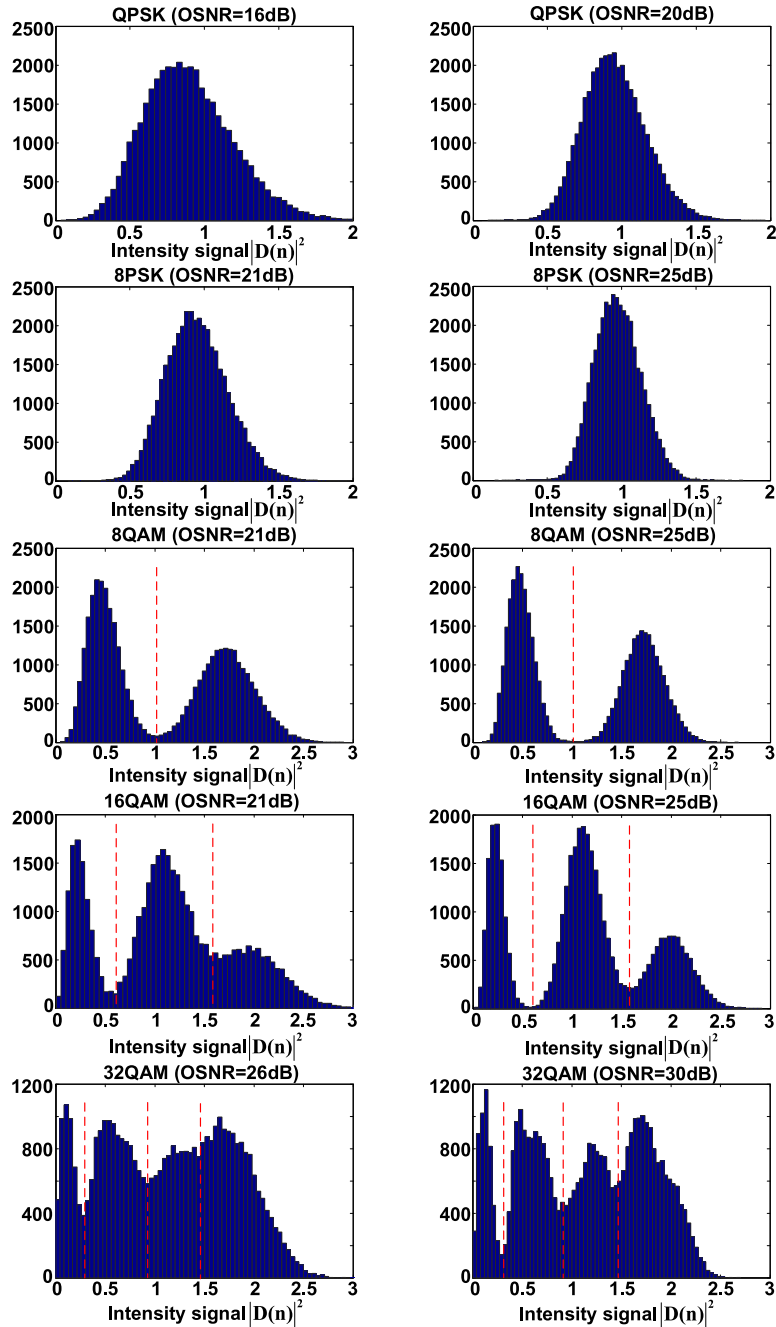


Fig. 3. Histograms of intensity signal  $|D(n)|^2$  of five commonly used modulation formats at different OSNR values.

It should be noted that individual Godard's error is a one-dimensional scalar. The calculated Godard's error may be slightly different in same OSNR case since the randomness of noise. If the Godard's error is close to that of adjacent OSNR, the deviation caused by the randomness of noise may lead to misjudgment. Compared with individual Godard's error, multiple Godard's errors as feature vector can alleviate this issue effectively. Therefore, initial data is partitioned. For instance, as the total number of symbols of QPSK signals is 24000, all symbols are divided into

three sections with 8000 symbols/section, and the Godard's error of each section is calculated independently. Therefore, the feature vector of QPSK signals is three-dimensional based on three independent values of calculated Godard's error. The dimension of feature vector of 8PSK signals is similar to that of QPSK signals. For  $m$ QAM signals, all symbols are also divided into three sections to calculate Godard's errors. However, 8QAM presents two intensity levels, where Godard's error needs to be calculated in each intensity level. Thus, the dimension of feature vector of 8QAM signals are 6. Similarly, the dimensions of feature vector of 16QAM and 32QAM signals are 9 and 12, respectively. For training vectors, the last additional element is the label containing the ordering information. As the Godard's error is obtained, the feature extraction is finished, then OSNR estimation is required.

## 2.2 Support Vector Ordinal Regression

SVOR, which is able to deal with special multi-classification problems with ordering information, is an extension version of traditional SVM. In the  $M$  (i.e.,  $M > 2$ ) classification problem, the training vectors are labeled with consecutive integers ordered from 1 to  $M$ . For instance,  $j$ -th class is only adjacent to  $(j - 1)$ -th class and  $(j + 1)$ -th class meanwhile not adjacent to any other classes. SVOR assumes that the distribution of the  $M$  classes can be separated by  $M - 1$  parallel discriminant hyperplanes. In fact, the features presented by adjacent OSNR are similar, so these features are easy to be confused and need to be distinguished. Therefore, SVOR generates parallel discriminant hyperplanes for adjacent classes is suitable for OSNR monitoring.

Essentially, the training set of SVOR is same as that of general multi-classification problems. The training set of SVOR can be denoted as:

$$T = \left\{ \mathbf{x}_i^j \right\}_{i=1,2,\dots,n}^{j=1,2,\dots,M}, \mathbf{x}_i^j \in \mathbb{R}^d \quad (2)$$

Where  $\mathbf{x}_i^j$  denotes  $i$ -th training vector of  $j$ -th class.  $n^j$  is the number of training vectors of  $j$ -th class. The superscript  $j$  is consecutive integer, and contains ordering information. Based on training set, SVOR attempts to find  $M - 1$  parallel discriminant hyperplanes. Under the condition that the thresholds are ordered, the parallel discriminant hyperplanes are defined by optimal mapping direction  $\mathbf{w}$ , and  $M - 1$  thresholds  $b_j$ .

$$\langle \mathbf{w} \cdot \phi(\mathbf{x}) \rangle = b_j \quad (3)$$

where,  $j = 1, 2, \dots, M-1$ .  $\phi(\mathbf{x})$  denotes the feature vector in a high dimensional reproducing kernel Hilbert space (RKHS) related to input vector  $\mathbf{x}$  of SVOR [25].  $\langle \cdot \cdot \rangle$  represents inner product. The schematic diagram of parallel discriminant hyperplanes is shown in Fig. 4.

As the extension version of SVM which is applied to two-classification problem, SVOR seeks to maximize the margin width between the nearest two classes of all adjacent classes based on training set. In order to obtain good generalization, SVOR allows some of the training vectors to be misclassified, and introduces slack variable. The function value  $f(\mathbf{x}_i^j) = \langle \mathbf{w} \cdot \phi(\mathbf{x}_i^j) \rangle$  of each training vector from the  $j$ -th class should be less than the lower margin  $b_j - 1$ , otherwise the error denoted as slack variable is defined as

$$\xi_i^j = \langle \mathbf{w} \cdot \phi(\mathbf{x}_i^j) \rangle - (b_j - 1) \quad (4)$$

Similarly, the function value of each training vector from  $(j + 1)$ -th class should be greater than the upper margin  $b_j + 1$ , otherwise the slack variable is calculated as

$$\xi_i^{j+1} = (b_j + 1) - \langle \mathbf{w} \cdot \phi(\mathbf{x}_i^{j+1}) \rangle \quad (5)$$

where the superscript  $*$  denotes that the error is associated with a training vector in the adjacent upper class of the  $j$ -th threshold [25].

In addition, penalty factor  $C$  ( $C > 0$ ), which represents the importance of the outlier data, needs to be set before training. Optimal penalty factor  $C$  can be obtained by cross-validation and

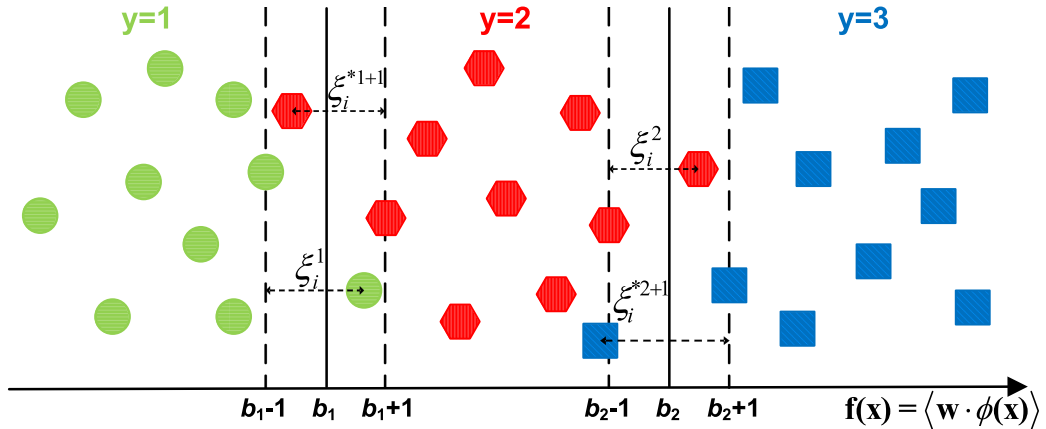


Fig. 4. The schematic diagram of parallel discriminant hyperplanes.

grid-search method. Based on slack variables and penalty factor, the primal problem of SVOR can be expressed as follows [25]:

$$\begin{aligned}
 \min_{\mathbf{w}, \mathbf{b}, \xi, \xi^*} \quad & \frac{1}{2} \langle \mathbf{w} \cdot \mathbf{w} \rangle + C \sum_{j=1}^M \sum_{i=1}^{n^j} (\xi_i^j + \xi_i^{*j}) \\
 \text{s.t.} \quad & \langle \mathbf{w} \cdot \phi(\mathbf{x}_i^j) \rangle - b_j \leq -1 + \xi_i^j, \xi_i^j \geq 0, \quad \forall i, j; \\
 & \langle \mathbf{w} \cdot \phi(\mathbf{x}_i^j) \rangle - b_{j-1} \geq 1 - \xi_i^{*j}, \xi_i^{*j} \geq 0, \quad \forall i, j; \\
 & b_{j-1} \leq b_j, \forall j.
 \end{aligned} \tag{6}$$

where auxiliary variables  $b_0 = -\infty$ ,  $b_M = +\infty$ . According to the Wolfe duality theory, the dual problem of the primal problem becomes a maximization problem involving the Lagrangian multipliers  $\mathbf{a} = (a_1^1, \dots, a_{n^1}^1, \dots, a_1^M, \dots, a_{n^M}^M)^T$ ,  $\mathbf{a}^* = (a_1^{*1}, \dots, a_{n^1}^{*1}, \dots, a_1^{*M}, \dots, a_{n^M}^{*M})^T$ , and  $\mu = (\mu^1, \dots, \mu^M)^T$  by introducing the KKT conditions into the Lagrangian function and applying the kernel trick  $\kappa(\mathbf{x}, \mathbf{x}') = \langle \phi(\mathbf{x}) \cdot \phi(\mathbf{x}') \rangle$  [25].

$$\begin{aligned}
 \max_{\mathbf{a}, \mathbf{a}^*, \mu} \quad & \sum_{j,i} (a_i^j + a_i^{*j}) - \frac{1}{2} \sum_{j,i} \sum_{j',i'} (a_i^{*j} - a_i^j) (a_{i'}^{*j'} - a_{i'}^j) \kappa(\mathbf{x}_i^j, \mathbf{x}_{i'}^{j'}) \\
 \text{s.t.} \quad & 0 \leq a_i^j \leq C, \quad \forall i, \forall j, \\
 & 0 \leq a_i^{*j+1} \leq C, \quad \forall i, \forall j, \\
 & \sum_{i=1}^{n^j} a_i^j + \mu^j = \sum_{i=1}^{n^{j+1}} a_i^{*j+1} + \mu^{j+1}, \forall j, \\
 & \mu^j \geq 0, \quad \forall j,
 \end{aligned} \tag{7}$$

where  $j = 1, 2, \dots, M-1$ . It should be noted that  $\mu^1, \mu^M, a_i^{*1}, a_i^M$  which are associated with  $b_0$  and  $b_M$  are always zero. The sequential minimal optimization (SMO) [26], [27] algorithm can be adapted for the solution of this convex quadratic programming problem depicted in Eq. (7). Then the optimal mapping direction  $\mathbf{w}$  can be calculated as:

$$\mathbf{w} = \sum_{j=1}^M \sum_{i=1}^{n^j} (a_i^{*j} - a_i^j) \phi(\mathbf{x}_i^j) \tag{8}$$

Furthermore, to obtain the thresholds  $b_j$ , the following steps for  $j = 1, 2, \dots, M - 1$  are carried out:

*Step 1:* Try to select a component  $a_i^j$  of  $\mathbf{a}$  which satisfies  $0 < a_i^j < C$ . If such a component can be selected,  $b_j$  can be defined as

$$b_j = 1 + \sum_{j'=1}^M \sum_{i'=1}^{n'} (a_{i'}^{*j'} - a_{i'}^j) \kappa(\mathbf{x}_{i'}^{j'}, \mathbf{x}_i^j) \quad (9)$$

Otherwise, turns to step 2;

*Step 2:* Try to select a component  $a_i^{*j+1}$  of  $\mathbf{a}^*$  which satisfies  $0 < a_i^{*j+1} < C$ . If such a component can be selected,  $b_j$  can be defined as

$$b_j = \sum_{j'=1}^M \sum_{i'=1}^{n'} (a_{i'}^{*j'} - a_{i'}^{j+1}) \kappa(\mathbf{x}_{i'}^{j'}, \mathbf{x}_i^{j+1}) - 1 \quad (10)$$

Otherwise, turns to step 3;

*Step 3:*  $b_j$  can be directly defined as

$$b_j = \frac{1}{2} (b_j^{low} + b_j^{up}) \quad (11)$$

$$\text{where } b_j^{low} = \max\{\max_{i \in I_1^j}(\mathbf{f}(\mathbf{x}_i^j) + 1), \max_{i \in I_4^j}(\mathbf{f}(\mathbf{x}_i^{j+1}) - 1)\}$$

$$b_j^{up} = \min \left\{ \min_{i \in I_3^j} (\mathbf{f}(\mathbf{x}_i^j) + 1), \min_{i \in I_2^j} (\mathbf{f}(\mathbf{x}_i^{j+1}) - 1) \right\}$$

$$I_1^j = \left\{ i \in \{1, 2, \dots, n^j\} \mid a_i^j = 0 \right\}, I_2^j = \left\{ i \in \{1, 2, \dots, n^{j+1}\} \mid a_i^{*j+1} = 0 \right\}$$

$$I_3^j = \left\{ i \in \{1, 2, \dots, n^j\} \mid a_i^j = C \right\}, I_4^j = \left\{ i \in \{1, 2, \dots, n^{j+1}\} \mid a_i^{*j+1} = C \right\}$$

When the optimal mapping direction  $\mathbf{w}$  and thresholds  $b_j$  are obtained, the discriminant function can be calculated as follow:

$$g(\mathbf{x}) = \min_{j \in \{1, \dots, M\}} \{j : \langle \mathbf{w} \cdot \phi(\mathbf{x}) \rangle - b_j < 0\} \quad (12)$$

After the training process is finished, the Eq. (12) is utilized to achieve classification of the new input vector  $\mathbf{x}$ .

### 3. Simulation Analysis

In order to verify the effectiveness of proposed OSNR monitoring method, numerical simulation has been implemented based on the VPI Transmission Maker. Throughout the numerical simulation, 28-Gbaud PDM-QPSK, PDM-8PSK, PDM-8QAM, PDM-16QAM and PDM-32QAM signals are generated and passed through an additive white Gaussian noise (AWGN) channel with variable OSNR. Since the OSNR threshold of QPSK signals corresponding to 7% forward error correction (FEC) is close to 12 dB, thus the OSNR monitoring range of QPSK signals is from 10 dB to 25 dB, while the OSNR monitoring ranges of 8PSK, 8QAM, 16QAM and 32QAM signals are from 15 dB to 30 dB. The step of variable OSNR is 1 dB. The proposed OSNR monitoring method is achieved in the off-line DSP module as shown in Fig. 1. For each modulation format, 80 testing vectors are applied at each OSNR value. The number of estimated OSNR for each modulation format is 16, so that 1280 testing vectors for each modulation format are employed to measure the accuracies of OSNR estimation.

To evaluate the influence of training data size, the accuracies of OSNR estimation with different number of training vectors for QPSK, 8PSK, 8QAM, 16QAM and 32QAM signals are shown in

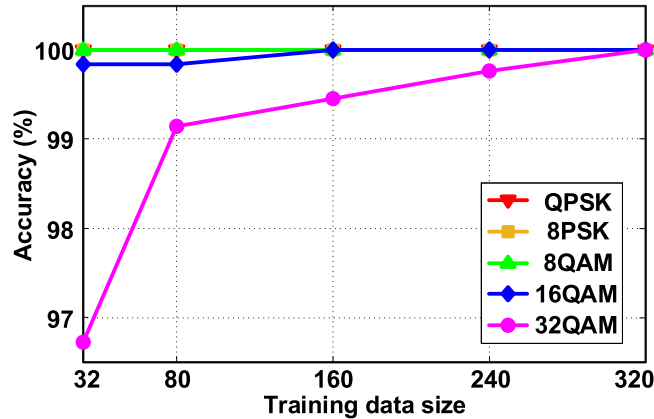


Fig. 5. Accuracy of OSNR estimation as a function of training data size for QPSK, 8PSK, 8QAM, 16QAM and 32QAM signals.

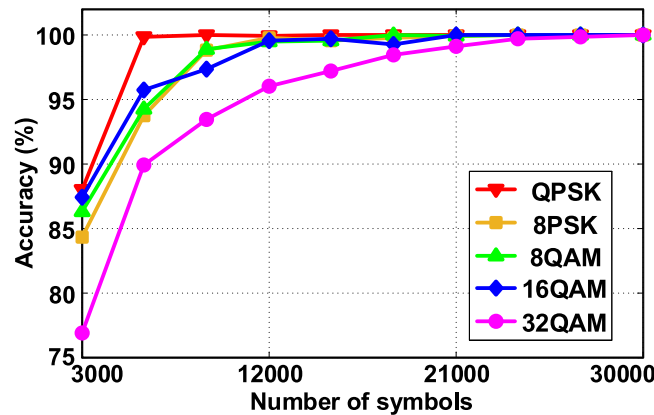


Fig. 6. Accuracy of OSNR estimation as a function of number of symbols for QPSK, 8PSK, 8QAM, 16QAM and 32QAM signals.

Fig. 5. The number of symbols of each training and testing vector for QPSK, 8PSK, 8QAM and 16QAM is 24000, while that of 32QAM is 30000. Compared with the features of higher order modulation formats such as 16QAM and 32QAM, the features of QPSK, 8PSK and 8QAM are more distinguishable. Therefore, it does not need too many training vectors to obtain the optimal mapping direction and thresholds. The proposed method achieves 100% accuracies for QPSK, 8PSK and 8QAM signals even if the number of training vectors is decreased to 2 at each OSNR value. So that the training data size is 32 (i.e.,  $2 \times 16 = 32$ ). Nevertheless, as the training data size of 16QAM and 32QAM signals is small, the mapping direction and thresholds are not optimized yet, resulting in relatively low accuracies; as the training data size grows, the mapping direction and thresholds are optimized, contributing to separate the testing vectors effectively. When the training data sizes rise to 160 and 320 for 16QAM and 32QAM signals respectively, error-free results are obtained.

The accuracies of OSNR estimation with different number of symbols for QPSK, 8PSK, 8QAM, 16QAM and 32QAM signals are shown in Fig. 6. Here, the optimized training data sizes (i.e., 32 for QPSK, 8PSK, 8QAM, 160 for 16QAM and 320 for 32QAM) obtained from Fig. 5 are applied in this test. If the number of symbols is not sufficient, a certain deviation of Godard's error caused by the randomness of noise may result in decreasing accuracy. As the number of symbols rises to 15000, error-free results are obtained for QPSK signals, while 8PSK, 8QAM and 16QAM signals require 24000, 24000 and 21000 symbols, respectively. Since the intensity levels of 32QAM signals is more

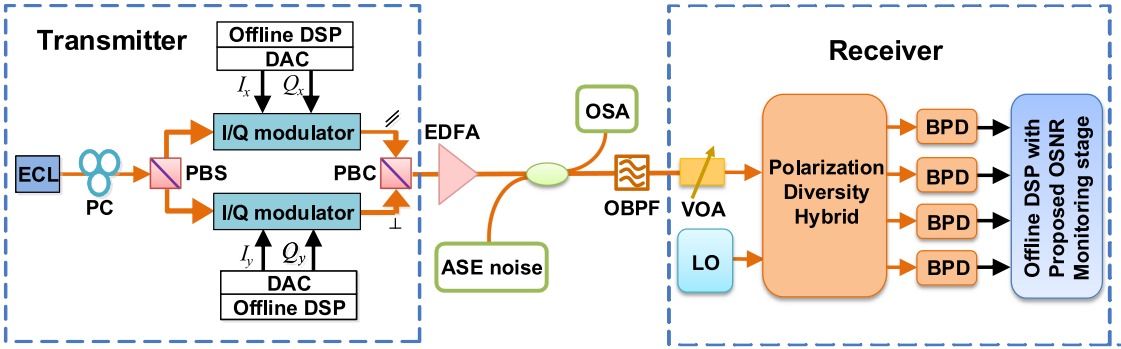


Fig. 7. Experimental setup of back-to-back coherent optical transmission system. PC: polarization controller; PBS: polarization beam splitter; PBC: polarization beam combiner; EDFA: erbium doped fiber amplifier; OBPF: optical band-pass filter; VOA: variable optical attenuator.

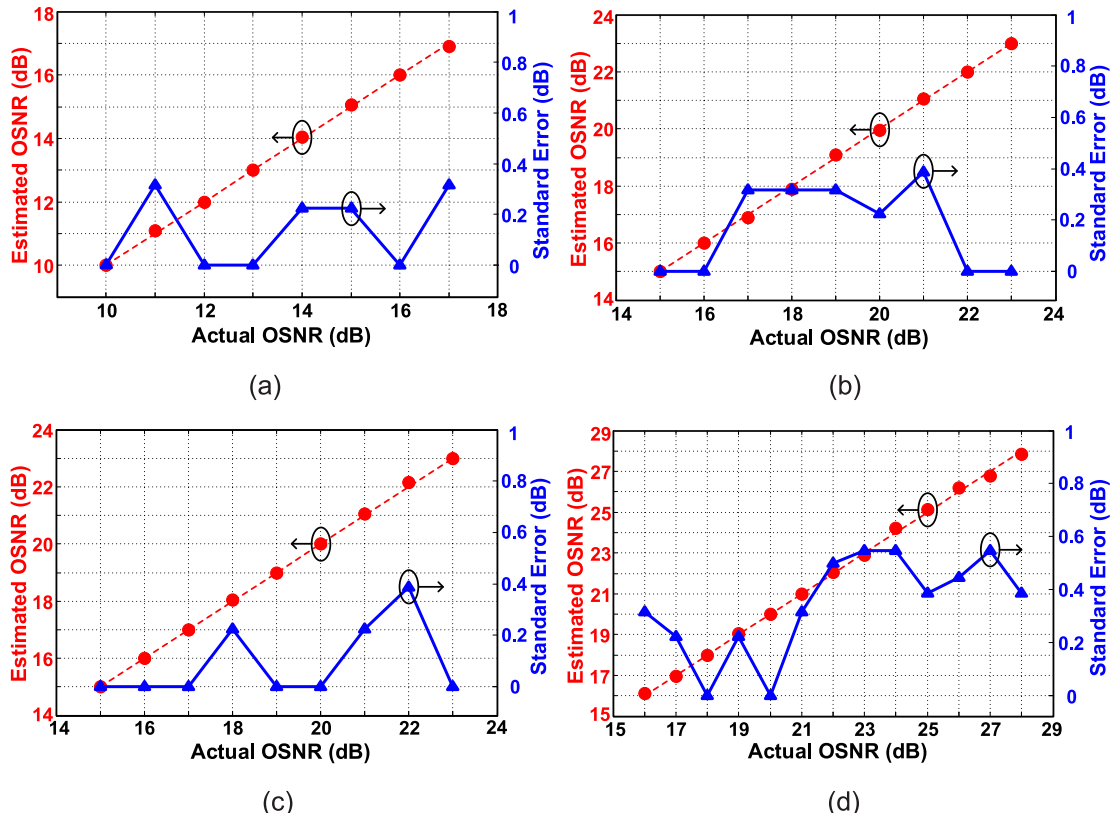


Fig. 8. Experimental results for OSNR estimation by SVOR: (a) QPSK; (b) 8PSK; (c) 8QAM and (d) 16QAM.

than that of other modulation formats, 32QAM signals also requires more symbols. The error-free result can be obtained as the number of symbols is increased to 30000.

#### 4. Experimental Verifications

In order to further demonstrate feasibility of our proposal, a proof-of-concept experiment has been performed. The experimental setup is shown in Fig. 7. At the transmitter side, a pseudo-random

bit sequence (PRBS) with a length of  $2^{15}-1$  is generated, and mapped into modulation format with 2 samples/ symbol. The up-sampled signals are shaped by using a square root raised cosine (SRRC) filter with a roll-off factor of 1.0. Next, a pre-distortion operation is utilized to overcome the frequency roll-off of a digital to analog converter (DAC). The light from an external cavity laser (ECL) at  $\sim 1550$ -nm with  $\sim 100$ -kHz linewidth is modulated by an integrated LiNbO<sub>3</sub> polarization-multiplexing I/Q modulator. The four branches of the modulator are driven by the DAC operating at 64-GSa/s and 25-GHz analog bandwidth for obtaining 28-Gbaud PDM-QPSK, PDM-8PSK, PDM-8QAM and PDM-16QAM signals. The received OSNR is measured by an optical spectra analyzer (OSA ANRITSU MS9740A) based on the out-of-band monitoring method. At the receiver, the modulated optical signals are combined with local oscillator (LO) at the polarization diversity hybrid, and then detected by the balanced photo-detector (BPD). Finally, the electrical signals are processed by off-line DSP module where the proposed OSNR monitoring method embedded.

In the experiment, the OSNR monitoring ranges for QPSK, 8PSK, 8QAM and 16QAM signals are 10 ~ 17 dB, 15 ~ 23 dB, 15 ~ 23 dB and 16 ~ 28 dB, respectively. The step of variable OSNR is 1 dB. The number of training vectors at each OSNR value for QPSK, 8PSK, 8QAM are both 5, while that of 16QAM is 30. For the four modulation formats, 20 testing vectors are employed at each OSNR value to validate accuracy of OSNR estimation. The number of symbols for the four modulation formats is 24000. The OSNR estimation results for QPSK, 8PSK, 8QAM and 16QAM signals are shown in Fig. 8. The red dots denote the averaged value of estimated OSNR over all testing vectors at each OSNR value [19], while the maximum errors are 0.1 dB, 0.1 dB, 0.15 dB and 0.2 dB for QPSK, 8PSK, 8QAM and 16QAM signals, respectively. It is important that the error of each OSNR estimation is kept within 1 dB for both four modulation formats, and could result in high level of reliability of OSNR monitoring. The blue triangles in Fig. 8 indicate standard errors at each OSNR value. The maximum standard errors for QPSK, 8PSK, 8QAM and 16QAM signals are 0.3162 dB, 0.3873 dB, 0.3873 dB and 0.5477 dB, respectively.

## 5. Conclusion

In this paper, an OSNR monitoring method based on SVOR is proposed for digital coherent receivers. The 100% estimation accuracies are firstly verified via numerical simulations with 28-Gbaud PDM-QPSK, PDM-8PSK, PDM-8QAM, PDM-16QAM and PDM-32QAM signals over a wide OSNR range. In addition, proof-of-concept experiment has also been implemented to demonstrate the feasibility among 28-Gbaud PDM-QPSK, PDM-8PSK, PDM-8QAM and PDM-16QAM signals. The errors of averaged values of estimated OSNR for all the signals are less than or equal to 0.2 dB.

---

## Reference

- [1] L. S. Yan, X. Liu, and W. Shieh, "Toward the Shannon limit of spectral efficiency," *IEEE Photon. J.*, vol. 3, no. 2, pp. 325–330, Apr. 2011.
- [2] O. Gerstel, M. Jinno, A. Lord, and S. J. B. Yoo, "Elastic optical networking: A new dawn for the optical layer?," *IEEE Commun. Mag.*, vol. 50, no. 2, pp. s12–s20, Feb. 2012.
- [3] A. P. T. Lau *et al.*, "Advanced DSP techniques enabling high spectral efficiency and flexible transmissions: Toward elastic optical networks," *IEEE Signal Process. Mag.*, vol. 31, no. 2, pp. 82–92, Mar. 2014.
- [4] S. J. Savory, "Digital coherent optical receivers: Algorithms and subsystems," *IEEE J. Sel. Top. Quantum Electron.*, vol. 16, no. 5, pp. 1164–1178, Sep. 2010.
- [5] Z. H. Dong, F. N. Khan, Q. Sui, K. P. Zhong, C. Lu, and A. P. T. Lau, "Optical performance monitoring: A review of current and future technologies," *J. Lightw. Technol.*, vol. 34, no. 2, pp. 525–543, Jan. 2016.
- [6] W. Y. Peng, L. X. Xi, X. Weng, X. Zhang, D. H. Zhao, and X. G. Zhang, "Novel in-band OSNR monitoring method based on polarization interference," *Chin. Opt. Lett.*, vol. 11, no. 8, Aug. 2013, Art. no. 080604.
- [7] M. R. Chitgarha *et al.*, "Demonstration of in-service wavelength division multiplexing optical signal to noise ratio performance monitoring and operating guidelines for coherent data channels with different modulation formats and various baud rates," *Opt. Lett.*, vol. 39, no. 6, pp. 1605–1608, Mar. 2014.
- [8] S. Oda *et al.*, "In-band OSNR monitor using an optical bandpass filter and optical power measurements for superchannel signals," in *Proc. Eur. Conf. Opt. Commun.*, 2013, Paper 3.12.
- [9] T. Saida *et al.*, "In-band OSNR monitor with high-speed integrated Stokes polarimeter for polarization division multiplexed signal," *Opt. Exp.*, vol. 20, no. 26, pp. 165–170, 2012.

- [10] L. Lundberg, H. Sunnerud, and P. Johannisson, "In-band OSNR monitoring of PM-QPSK using the Stokes parameters," in *Proc. Opt. Fiber Commun. Conf.*, 2015, @@ W4D. 5.
- [11] D. J. Ives, B. C. Thomsen, R. Maher, and S. Savory, "Estimating OSNR of equalised QPSK signals," in *Proc. Eur. Conf. Opt. Commun.*, Geneva, Switzerland, 2011, Paper Tu.6.A.6.
- [12] M. S. Faruk, Y. Mori, and K. Kikuchi, "In-band estimation of optical signal-to-noise ratio from equalized signals in digital coherent receivers," *IEEE Photon. J.*, vol. 6, no. 1, pp. 1–9, Feb. 2014.
- [13] C. Zhu *et al.*, "Statistical moments-based OSNR monitoring for coherent optical systems," *Opt. Exp.*, vol. 20, no. 16, pp. 17711–17721, Jul. 2012.
- [14] F. Pittala, F. N. Hauske, Y. Ye, N. G. Gonzalez, and I. T. Monroy, "Joint PDL and in-band OSNR monitoring supported by data-aided channel estimation," in *Proc. Opt. Fiber Commun. Conf.*, Los Angeles, CA, USA, Mar. 2012, Paper OW4G.
- [15] R. Schmogrow *et al.*, "Error vector magnitude as a performance measure for advanced modulation formats," *IEEE Photon. Technol. Lett.*, vol. 24, no. 1, pp. 61–63, Jan. 2012.
- [16] C. Do, A. V. Tran, C. Zhu, D. Hewitt, and E. Skafidas, "Data-aided OSNR estimation for QPSK and 16-QAM coherent optical system," *IEEE Photon. J.*, vol. 5, no. 5, Oct. 2013, Art. no. 6601609.
- [17] X. Lin, O. A. Dobre, T. M. N. Ngatched, Y. A. Eldemerdash, and C. Li, "Joint modulation classification and OSNR estimation enabled by support vector machine," *IEEE Photon. Technol. Lett.*, vol. 30, no. 24, pp. 2127–2130, Dec. 2018.
- [18] F. N. Khan *et al.*, "Joint OSNR monitoring and modulation format identification in digital coherent receivers using deep neural networks," *Opt. Exp.*, vol. 25, no. 15, pp. 17767–17776, Jul. 2017.
- [19] D. S. Wang, M. Zhang, J. Li, Z. Li, J. Qiang Li, C. Song, and X. Chen, "Intelligent constellation diagram analyzer using convolutional neural network-based deep learning," *Opt. Exp.*, vol. 25, no. 15, pp. 17150–17166, Jul. 2017.
- [20] D. Godard, "Self-recovery equalization and carrier tracking in two-dimensional data communication systems," *IEEE Trans. Commun.*, vol. 28, no. 11, pp. 1867–1875, Nov. 1980.
- [21] M. Kuschnerov, F. N. Hauske, K. Piyawanno, B. Spinnler, A. Napoli and B. Lankl, "Adaptive chromatic dispersion equalization for non-dispersion managed coherent systems," in *Proc. Opt. Fiber Commun. Conf.*, San Diego, CA, USA, 2009, Paper OMT1.
- [22] L. Jiang *et al.*, "Low complexity and adaptive nonlinearity estimation module based on Godard's error," *IEEE Photon. J.*, vol. 8, no. 1, Feb. 2016, Art. no. 7801007.
- [23] L. Jiang *et al.*, "Chromatic dispersion, nonlinear parameter, and modulation format monitoring based on Godard's error for coherent optical transmission systems," *IEEE Photon. J.*, vol. 10, no. 1, pp. 1–12, Feb. 2018.
- [24] L. Jiang *et al.*, "Robust and blind modulation format identification for elastic optical networks," *Eur. Conf. Opt. Commun.*, Rome, Italy, 2018, Paper We.2.20.
- [25] W. Chu and S. S. Keerthi, "Support vector ordinal regression," *Neural Comput.*, vol. 19, no. 3, pp. 792–815, 2007.
- [26] Platt and J. C., "Fast training of support vector machines using sequential minimal optimization," in *Advances in Kernel Methods -Support Vector Learning 12*. Cambridge, MA, USA: MIT Press, 1999, pp. 185–208.
- [27] Keerthi, S. S., S. K. Shevade, C. Bhattacharyya, and K. R. K. Murthy, "Improvements to Platt's SMO algorithm for SVM classifier design," *Neural Comput.*, vol. 13, pp. 637–649, Mar. 2001.